

Influence of Ni doping on the electronic structure of Ni₂MnGa

Aparna Chakrabarti,¹ C. Biswas,² S. Banik,² R. S. Dhaka,² A. K. Shukla,² and S. R. Barman^{2,*}

¹*Solid State Laser Division, Centre for Advanced Technology, Indore, 452013, Madhya Pradesh, India*

²*UGC-DAE Consortium for Scientific Research, University Campus, Khandwa Road, Indore, 452017, Madhya Pradesh, India*

(Received 12 May 2005; published 5 August 2005)

The modifications in the electronic structure of Ni_{2+x}Mn_{1-x}Ga by Ni doping have been studied using the full potential linearized augmented plane wave method and ultraviolet photoemission spectroscopy. Ni 3*d*-related electron states appear due to formation of Ni clusters. We show the possibility of changing the minority-spin density of states (DOS) with Ni doping, while the majority-spin DOS remains almost unchanged. The total magnetic moment decreases with excess Ni. The total energy calculations corroborate the experimentally reported changes in the Curie temperature and the martensitic transition temperature with *x*.

DOI: [10.1103/PhysRevB.72.073103](https://doi.org/10.1103/PhysRevB.72.073103)

PACS number(s): 79.60.-i, 71.20.Lp

Ni₂MnGa is an unique material because it exhibits both ferromagnetism and shape memory effect and is an ideal candidate for magnetically controlled shape memory applications.^{1,2} The highest known magnetic-field-induced strain, giant magnetocaloric effect, and large negative magnetoresistance have been reported in Ni-Mn-Ga.¹⁻⁵ Physical properties of Ni₂MnGa are highly composition dependent. It is reported that replacing Mn by Ni in Ni_{2+x}Mn_{1-x}Ga for *x* = 0 to 0.2 causes the Curie temperature (*T_C*) to decrease from 376 K to 325 K and the martensitic transition temperature (*T_M*) to increase from 210 K to 325 K.^{6,7} These interesting properties make Ni_{2+x}Mn_{1-x}Ga a very important system for both fundamental physics and technological applications.

The explanation of the above-mentioned characteristics of Ni-doped Ni₂MnGa is related to its electronic structure. So, in this paper we investigate the electronic structure of Ni_{2+x}Mn_{1-x}Ga using ultraviolet photoemission spectroscopy (UPS) and full potential linearized augmented plane wave (FPLAPW) calculations. Different band structure studies on Ni₂MnGa and related Heusler alloys in literature deal with the stoichiometric composition;⁸⁻¹⁴ but very few study the effect of Ni doping.^{15,16} Recently, Enkovaara *et al.* showed that in Mn-rich Ni₂MnGa, the doped Mn atoms are antiferromagnetically aligned.¹⁵ MacLaren calculated the density of states (DOS) for 20% Ni-rich Ni₂MnGa using the layer Korringa-Kohn-Rostoker (KKR) method and correlated the structural properties with DOS.¹⁶

The *ab initio* relativistic spin-polarized FPLAPW calculations were performed using the WIEN97 code¹⁷ with the generalized gradient approximation¹⁸ for exchange correlation. An energy cutoff for the plane wave expansion of 16 Ry and *l_{max}* = 10 were used. The muffin-tin radii were taken to be Ni 1.19 Å, Mn 1.27 Å, and Ga 1.19 Å. The number of *k* points in the irreducible Brillouin zone (BZ) for self-consistent-field cycles and DOS calculation varied between 147 and 168 for different structures. For the *x* = 0 tetragonal martensitic phase, the calculations were performed with the experimentally determined lattice constants: *a* = *b* = 5.92 Å, *c* = 5.56 Å, space group *Fmmm* (*Z* = 4) with atomic positions 8*f* (Ni), 4*b* (Mn), and 4*a* (Ga) without considering modulation.^{19,20} The FPLAPW calculation has also been performed with the real structure with seven-layer modulation²¹ in the *P_{nm}* space

group (*Z* = 14) with *a* = 4.215 Å, *b* = 29.302 Å, and *c* = 5.557 Å with 80 *k* points in the irreducible BZ and is indicated in text as *x* = 0*M*. For Ni_{2.25}Mn_{0.75}Ga, our x-ray diffraction (XRD) studies do not show any modulation²² and this is in agreement with literature.²³ So, for Ni excess Ni_{2.25}Mn_{0.75}Ga, calculations were performed by replacing a Mn by Ni in the nonmodulated *Fmmm* structure and with the same lattice constants as *x* = 0 (henceforth designated as *x* = 0.25). Calculation was also performed in the same structure but with the actual lattice constants of Ni_{2.25}Mn_{0.75}Ga (*a* = *b* = 5.439 Å, *c* = 6.563 Å, and *c/a* = 1.2).²² This is henceforth referred to as *x* = 0.25(1.2). The number 1.2 in the parentheses is the *c/a* value. All the DOS calculations shown here are done in the ferromagnetic ground state.^{5-7,24}

Polycrystalline ingots of Ni_{2+x}Mn_{1-x}Ga were prepared by standard procedure.⁶ Our XRD, differential scanning calorimetry (DSC), resistivity results agree with literature.^{6,19,20,23} The energy dispersive analysis of x rays shows that the samples are homogeneous. The intended and actual compositions agree well, e.g., Ni_{2.02}Mn_{0.97}Ga_{1.02} and Ni_{2.21}Mn_{0.78}Ga_{1.01} for *x* = 0 and 0.2, respectively. He I UPS (*hν* = 21.2 eV) was performed at a base pressure of 6 × 10⁻¹¹ mbar using an electron energy analyzer from Specs GmbH, Germany. The samples were mechanically scraped to expose fresh surfaces devoid of oxygen and carbon contamination.

The atomic photoemission cross sections of Ni 3*d* and Mn 3*d* at *hν* = 21.2 eV are 4.0 and 5.3 Mb, respectively.²⁵ These values are an order of magnitude higher than that of Ni 4*s*, Mn 4*s*, and Ga 4*s*, *p* states.²⁵ So, the UPS valence band (VB) spectra are calculated by adding the partial DOS (PDOS) of Ni and Mn 3*d*, multiplied by their respective photoemission cross sections.²⁶ This added DOS is multiplied with the Fermi function at the measurement temperature and convoluted with a Voigt function. The full width at half maximum (FWHM) of the Gaussian component (≈ 100 meV) of the Voigt function represents the instrumental resolution. The energy-dependent Lorentzian FWHM that represents the lifetime broadening is 0.3*E*, where *E* is the energy with respect to *E_F*.²⁷

We compare the experimental UPS spectrum of Ni₂MnGa in the martensitic phase with the calculated VB of both non-

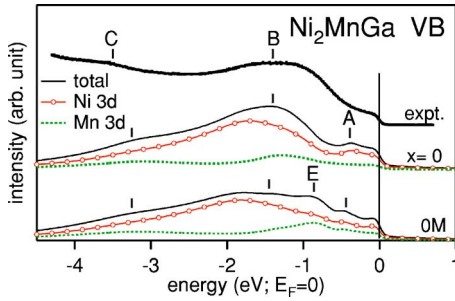


FIG. 1. (Color online) VB spectra of Ni_2MnGa ($x=0$) in the martensitic phase from He I ultraviolet photoemission (black dots) and FPLAPW calculation (black solid line). Ni 3d (red solid line with open circles) and Mn 3d (green dashed line) contributions to the calculated VB are shown. The spectra are staggered.

modulated ($x=0$) and modulated ($x=0M$) structures in Fig. 1. The UPS spectrum exhibits a broad main peak centered at -1.4 eV (B) and a weak feature at -3.5 eV (C). The cutoff at 0 eV is the Fermi level (E_F). The shape of B [corresponding DOS feature is B' in Fig. 2(b)] of $x=0$ is in good agreement with the UPS spectrum. The VB is largely dominated by Ni 3d states with peak at -1.75 eV. Mn 3d states exhibit two features at -1.3 and -3.1 eV. Feature C arises due to Ni 3d–Mn 3d bonding and is related to feature C' in the DOS [Fig. 2(b)]. Features A , B , and C appear at similar energies in $x=0$ and $0M$. This is expected because, although $0M$ has a large orthorhombic unit cell, modulation involves a small (0% to 5%) periodic shuffle of the (110) atomic planes of the nonmodulated structure along the $[1\bar{1}0]$ direction²⁸. However, in $0M$ VB, a feature E appears prominently, which has hardly any signature in the experimental spectrum. This feature is related to Mn 3d–Ni 3d hybrid states that are more intense and appear at -0.9 eV, in contrast to $x=0$ VB. It is evident from Fig. 1 that $x=0$ VB is in better agreement with

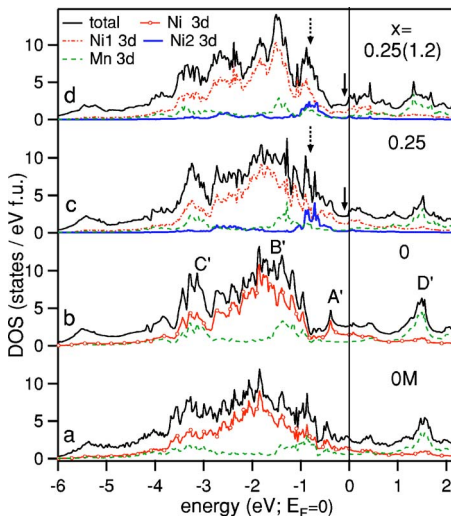


FIG. 2. (Color online) Total DOS (black solid line) and Ni 3d [red solid line with open circles for (a) and (b); red dot-dashed line and blue thick solid line for (c) and (d), see text] and Mn 3d (green dashed line) partial DOS of ferromagnetic $\text{Ni}_{2+x}\text{Mn}_{1-x}\text{Ga}$ in the martensitic phase.

experiment than $0M$ VB. The possible reasons could be (i) mean free path of photoelectrons in UPS is 10 – 15 Å, hence UPS probes the $0M$ structure ($b \approx 29$ Å) only partially; (ii) due to possible surface relaxation or reconstruction effects, the modulated structure is modified or absent at the surface. The Ni 3d related feature A at -0.4 eV [feature A' in Fig. 2(b)] is absent in the experiment. A similar discrepancy between UPS and the calculated VB has been reported for other Mn-based Heusler alloys²⁶ and the possible reasons are discussed later.

To investigate the effect of Ni doping only, we compare the $x=0$ and 0.25 DOS in Fig. 2(b) and 2(c), both with lattice constants of $x=0$. In both cases, the DOS is dominated by Ni and Mn 3d bonding states (B' and C'), as in other related Heusler alloys.^{8,10} The occupied Mn 3d PDOS is split into clearly separated e_g and t_{2g} states, appearing at -1.3 and -3 eV, respectively. Feature D' in the antibonding region above E_F is largely dominated by Mn 3d PDOS. An interesting difference between $x=0$ and 0.25 is observed around -0.8 eV, where new electron states appear in the latter (dashed arrow) that fill up the valley between A' and B' in $x=0$. The PDOS of Ni2, i.e., the doped Ni atom in Mn position, has its maximum at 0.8 eV. 3d PDOS of Ni1 (Ni atoms in Ni position) also appear at this energy with similar intensity. This shows that these states arise from the bonding between doped and existing Ni atoms. In fact, since the nearest neighbor (NN) of a Mn atom is eight Ni atoms, when Mn is replaced by Ni, a nine-atom body-centered-tetragonal Ni cluster is formed with a NN distance of 2.53 Å. Hence, Ni–Ni bonding occurs at the expense of Ni–Mn bonding. To test this explanation, we have calculated the DOS of $\text{Ni}_2\text{Mn}_{0.75}\text{Ga}_{1.25}$ where, instead of Ni, Ga replaces Mn. As expected, the DOS does not show the Ni-related extra states because in this case Ni clustering does not occur.²⁹

The change in electronic structure in the Ni-doped case between the real structure [$x=0.25(1.2)$, $c/a=1.2$] and non-equilibrium $x=0.25$ structure ($c/a=0.94$) is shown in Figs. 2(c) and 2(d). The total energy (E_{tot}) calculated using FPLAPW confirm that $0.25(1.2)$ is more stable than 0.25 by 12.2 meV/atom. In $0.25(1.2)$, the Ni 3d-related new states appear as a clear peak at -0.8 eV. The Ni1 3d states are more intense than the Ni2 3d states. The Mn 3d-related feature D' is broadened. A comparison of Figs. 2(a) and 2(d) shows the difference between the DOS of undoped ($0M$) and Ni-doped Ni_2MnGa [$0.25(1.2)$], both with actual experimentally determined structures. In $0M$, Ni 3d–Mn 3d hybrid states are observed around 0.9 eV that gives rise to feature E in Fig. 1. In contrast, in $0.25(1.2)$, Ni1 3d–Ni2 3d hybrid states dominate this region.

A dip is observed in the $x=0.25$ DOS in the near E_F region between A' and E_F (black arrow, Fig. 2). To understand its origin, the spin-projected DOS in the near E_F region is shown in Fig. 3(a). We find that the dip is due to a decrease in the minority-spin DOS near E_F by 31% in $x=0.25$ with respect to $x=0$ (from 1.6 to 1.1 states/eV f.u. at -0.15 eV). If compared to $0M$, the decrease is even larger (41%). Because of Ni doping, there is a redistribution of the partially filled minority-spin DOS. Both Ni and Mn 3d PDOS decrease in the near E_F region resulting in the dip,

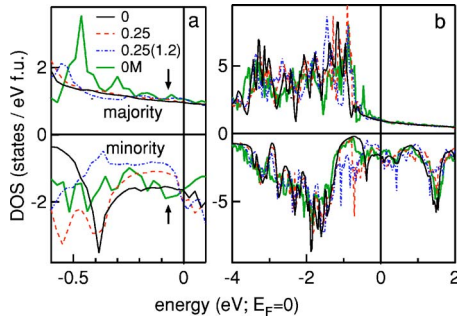


FIG. 3. (Color online) Spin-projected DOS of $\text{Ni}_{2+x}\text{Mn}_{1-x}\text{Ga}$ (a) in near E_F (b) extended region for $x=0$ (black solid line), 0.25 (red dashed line), 0.25(1.2) (blue dot-dashed line), and 0M (green thick solid line).

while new Ni1-Ni2 hybrid states appear around -0.8 eV. The minority-spin DOS is further reduced by 43% in 0.25(1.2) compared to $x=0$, and with respect to 0M the decrease is 55% [Fig. 3(a)]. In 0.25(1.2), feature A' is absent and the dip is more pronounced and broadened (~ 0.55 eV to E_F). In contrast, the majority-spin DOS near E_F remains essentially unchanged in all cases [arrow, Fig. 3(a)], because they are almost fully filled.¹⁶ Thus, $\text{Ni}_{2+x}\text{Mn}_{1-x}\text{Ga}$ presents an exciting possibility of tuning the minority-spin DOS near E_F with Ni doping, which might have interesting implications in spin-polarized transport. Comparing Figs. 2 and 3(b), we find that D' originates predominantly from Mn 3d minority-spin states, while Mn 3d majority-spin states are almost fully occupied. This is the reason why Mn has a large magnetic moment. Features B' and A' are dominated by minority-spin states in all cases, except for 0M where A' is broader and has similar contributions from both spin states. Feature C' is dominated by majority-spin states.

UPS VB spectra in Fig. 4 show that the main peak of $\text{Ni}_{2.1}\text{Mn}_{0.9}\text{Ga}$ ($x=0.1$) is centered at -1.1 eV with a shoulder at -1.65 eV, (in contrast to Ni_2MnGa). For $\text{Ni}_{2.2}\text{Mn}_{0.8}\text{Ga}$ ($x=0.2$), the -1.1 eV peak becomes relatively more intense and shifts to -0.9 eV. The experimental difference spectrum between $x=0.2$ and 0 shows extra states in the former around -0.65 eV. The difference spectrum from theory between $x=0.25(1.2)$ and 0 exhibits a peak at -0.75 eV in agreement with experiment and these extra states are the new Ni1

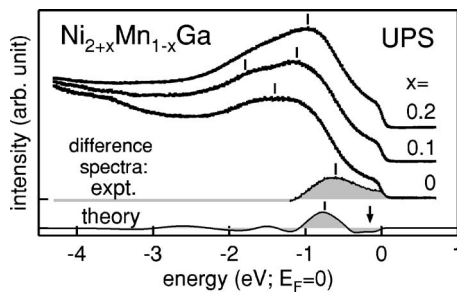


FIG. 4. UPS spectra of $\text{Ni}_{2+x}\text{Mn}_{1-x}\text{Ga}$ in the martensitic phase. The spectra have been normalized to the same height and staggered along the vertical axis. The experimental (between $x=0.2$ and 0) and calculated (between $x=0.25(1.2)$ and $x=0$) difference spectra are shown.

-Ni2 3d bonding states, as discussed earlier (Fig. 2). The agreement is not good if the 0M VB is used to calculate the theoretical difference spectrum (not shown in Fig. 4) and this supports our contention that the surface electronic structure is hardly influenced by modulation. The dip in the DOS between -0.4 eV and E_F is observed in the theoretical difference spectrum (arrow, Fig. 4), but is not clearly observed from experiment. Possible reasons for this disagreement could be surface relaxation or the presence of antisite defects,³⁰ etc. To find the effect of surface relaxation, we have calculated the $x=0.25$ DOS with 10% lattice expansion. We find that the dip region shifts to E_F ,²⁹ which would imply absence of the dip below E_F in UPS. Also, absence of feature A (Fig. 1) in UPS is explained by the shift in the DOS. We have calculated the DOS of $x=0.25$ with a simple antisite defect (Ni and Mn positions interchanged). The DOS does not show the dip and feature A' is absent. Thus, surface relaxation and/or antisite defects are likely to be responsible for the present and similar earlier²⁶ discrepancies between experiment and theory.

Now we turn to the discussion of the bulk magnetic moments calculated using FPLAPW for the real structures. The total magnetic moment for Ni_2MnGa (0M) is $3.81\mu_B$, and the local moments per site for Mn, Ni, and Ga are 3.06 , 0.21 , and $-0.03\mu_B$, respectively. These magnetic moments are in better agreement with experiment³¹ compared to $x=0$ (total: $4.13\mu_B$, Mn: $3.44\mu_B$, and Ni: $0.36\mu_B$). Thus, the magnetic moment, which is a bulk property, is better described by the 0M structure. For $x=0.25(1.2)$, the total magnetic moment is $3.31\mu_B$, and the local moments per site for Ni1, Ni2, Mn, and Ga are 0.37 , 0.23 , 3.41 , and $-0.03\mu_B$, respectively. The doped Ni2 is in ferromagnetic configuration, and its moment is smaller than Ni1. Although the Mn moment increases with Ni doping, the total moment decreases because the Ni2 moment is less than that of the Mn it replaces. Magnetization measurements also show a decrease in total saturation moment with excess Ni.²⁴

For Ni_2MnGa , the ferromagnetic (FM) transition occurs in the austenitic phase since $T_C > T_M$. So, to find the stability of the FM state, the difference in E_{tot} between the paramagnetic (PM) and the FM state (ΔE_{tot}) has been calculated in the austenitic phase. We find ΔE_{tot} to be 322 meV/atom for Ni_2MnGa . In contrast, our recent DSC studies on $\text{Ni}_{2.25}\text{Mn}_{0.75}\text{Ga}$ show that $T_M > T_C$ and the magnetic transition occurs in the martensitic phase,²² and ΔE_{tot} turns out to be 219 meV/atom. Since Ni_2MnGa satisfies the Stoner condition of ferromagnetism, it is possible to approximately relate T_C to ΔE_{tot} by $k_B T_C \sim \Delta E_{\text{tot}}$.^{9,11} Although this expression gives a much higher value of T_C ,¹¹ it could be used to find the relative variation. Thus, with respect to T_C ($=376$ K) of $x=0$; for 0.25(1.2) T_C should be 256 K. So, from theory we find that T_C decreases with Ni doping, which explains the experimental data.^{6,7,24}

In order to relate T_M to x , we note that E_{tot} for the martensitic phase should be lower than the austenitic phase, since the former is the lower-temperature phase. A higher total energy difference between the two phases (δE_{tot}) would imply greater stability of the latter and hence enhanced T_M . For NiTi and PdTi this is indeed found to be so.³² For

Ni_2MnGa in the FM state, δE_{tot} is 3 meV/atom. For $x = 0.25(1.2)$ in the PM state, δE_{tot} is 39 meV/atom. Thus, the martensitic phase is more stable compared to the austenitic phase in 0.25(1.2), i.e., the Ni-doped case. This is consistent with the experimentally observed higher T_M with Ni doping.^{6,7,22}

In conclusion, based on FPLAPW calculations and photoemission spectroscopy, we show that with Ni doping new Ni-related electron states appear due to formation of Ni clusters in $\text{Ni}_{2+x}\text{Mn}_{1-x}\text{Ga}$. The reported trends in the variation of T_C , T_M , and magnetic moments with x are explained. For Ni_2MnGa , the effect of modulation in the structure is not evident at the surface, while bulk property like magnetic moment is better described by the modulated $0M$ structure. A

lthough not clearly observed in the spin-integrated UPS spectra possibly due to surface relaxation or antisite defects, we find that with Ni doping a dip appears below E_F in the minority-spin DOS calculated using FPLAPW. In contrast, the majority-spin DOS remains unchanged. This indicates a probable future application of $\text{Ni}_{2+x}\text{Mn}_{1-x}\text{Ga}$ in spin-polarized transport with tunable efficiency through controlled doping.

We thank K. C. Rustagi, T. P. S. Nathan, P. Chaddah, and A. Gupta for constant encouragement. N. P. Lalla, A. M. Awasthi, and R. Rawat are thanked for providing sample characterization facilities, and S. C. Das is thanked for technical help. S.B. and A.K.S. acknowledge the financial support from D.S.T.

*Corresponding author. Electronic address: srbarman@mailcity.com, barman@csr.ernet.in

¹S. J. Murray, M. Marioni, S. M. Allen, R. C. O'Handley, and T. A. Lograsso, *Appl. Phys. Lett.* **77**, 886 (2000).

²A. Sozinov, A. A. Likhachev, N. Lanska, and K. Ullakko, *Appl. Phys. Lett.* **80**, 1746 (2002).

³J. Marcos, L. Mañosa, A. Planes, F. Casanova, X. Batlle, and A. Labarta, *Phys. Rev. B* **68**, 094401 (2003).

⁴X. Zhou, W. Li, H. P. Kunkel, and G. Williams, *J. Phys.: Condens. Matter* **16**, L39 (2004).

⁵C. Biswas, R. Rawat, and S. R. Barman, *Appl. Phys. Lett.* **86**, 202508 (2005).

⁶A. N. Vasil'ev, A. D. Bozhko, V. V. Khovailo, I. E. Dikshtein, V. G. Shavrov, V. D. Buchelnikov, M. Matsumoto, S. Suzuki, T. Takagi, and J. Tani, *Phys. Rev. B* **59**, 1113 (1999).

⁷F. Zuo, X. Su, P. Zhang, G. C. Alexzandrakis, F. Yang, and K. H. Wu, *J. Phys.: Condens. Matter* **11**, 2821 (1999).

⁸J. Kübler, A. R. Williams, and C. B. Sommers, *Phys. Rev. B* **28**, 1745 (1983).

⁹S. Fujii, S. Ishida, and S. Asano, *J. Phys. Soc. Jpn.* **58**, 3657 (1989).

¹⁰W. Lin and A. J. Freeman, *Phys. Rev. B* **45**, 61 (1992).

¹¹O. I. Velikokhatnyi and I. I. Nuamov, *Phys. Solid State* **41**, 617 (1999).

¹²A. Ayuela, J. Enkovaara, K. Ullakko, and R. M. Nieminen, *J. Phys.: Condens. Matter* **11**, 2017 (1999); A. Ayuela, J. Enkovaara, and R. M. Nieminen, *J. Phys.: Condens. Matter* **14**, 5325 (2002).

¹³C. Bungaro, K. M. Rabe, and A. Dal Corso, *Phys. Rev. B* **68**, 134104 (2003).

¹⁴A. T. Zayak, P. Entel, J. Enkovaara, and R. M. Nieminen, *J. Phys.: Condens. Matter* **15**, 159 (2003).

¹⁵J. Enkovaara, O. Heczko, A. Ayuela, and R. M. Nieminen, *Phys. Rev. B* **67**, 212405 (2003); J. Enkovaara, A. Ayuela, J. Jalkanen, L. Nordström, and R. M. Nieminen, *Phys. Rev. B* **67**, 054417 (2003).

¹⁶J. M. MacLaren, *J. Appl. Phys.* **91**, 7801 (2002).

¹⁷P. Blaha, K. Schwartz, and J. Luitz, WIEN97 (Karlheinz Schwarz, Tech. Universität, Wien, Austria, 1999).

¹⁸J. P. Perdew, K. Burke, and M. Ernzerhof, *Phys. Rev. Lett.* **77**, 3865 (1996).

¹⁹P. J. Webster, K. R. A. Ziebeck, S. L. Town, and M. S. Peak, *Philos. Mag. B* **49**, 295 (1984).

²⁰B. Wedel, M. Suzuki, Y. Murakami, C. Wedel, T. Suzuki, D. Shindo, and K. Itagaki, *J. Alloys Compd.* **290**, 137 (1999).

²¹P. J. Brown, J. Crangle, T. Kanomata, M. Matsumoto, K.-U. Neumann, B. Ouladdiaf, and K. R. A. Ziebeck, *J. Phys.: Condens. Matter* **14**, 10159 (2002).

²²S. Banik, C. Biswas, and S. R. Barman (unpublished).

²³J. Pons, V. A. Chernenko, R. Santamarta, and E. Cesari, *Acta Mater.* **48**, 3027 (2000); N. Lanska, O. Söderberg, A. Sozinov, Y. Ge, K. Ullakko and V. K. Lindroos, *J. Appl. Phys.* **95**, 8074, 2004.

²⁴F. Albertini, L. Pareti, A. Paoluzi, L. Morellon, P. A. Algarabel, M. R. Ibarra, and L. Righi, *Appl. Phys. Lett.* **81**, 4032 (2002).

²⁵J. J. Yeh and I. Lindau, *At. Data Nucl. Data Tables* **32**, 1 (1985).

²⁶D. Brown, M. D. Crapper, K. H. Bedwell, M. T. Butterfield, S. J. Guilfoyle, A. E. R. Malins, and M. Petty, *Phys. Rev. B* **57**, 1563 (1998).

²⁷A. Fujimori, and F. Minami, *Phys. Rev. B* **30**, 957 (1984); S. R. Barman and D. D. Sarma, *Phys. Rev. B* **51**, 4007 (1995); D. D. Sarma, N. Shanthi, S. R. Barman, N. Hamada, H. Sawada, and K. Terakura, *Phys. Rev. Lett.* **75**, 1126 (1995).

²⁸V. V. Martynov and V. V. Kokorin, *J. Phys. III* **2**, 739 (1992).

²⁹A. Chakrabarti, S. Banik and S. R. Barman (unpublished).

³⁰P. Larson, S. D. Mahanti, and M. G. Kanatzidis, *Phys. Rev. B* **62**, 12754 (2000).

³¹P. J. Brown, A. Y. Bargawi, J. Crangle, K.-U. Neumann, and K. R. A. Ziebeck, *J. Phys.: Condens. Matter* **11**, 4715 (1999).

³²G. Bihlmayer, R. Eibler, and A. Neckel, *Philos. Mag. B* **73**, 511 (1996).